J|A|C|S
ARTICLES
Published on Web 09/23/2004

Synthesis, Characterization, and Framework Heteroatom Localization in ITQ-21

Teresa Blasco,[†] Avelino Corma,*[,†] Maria José Díaz-Cabañas,[†] Fernando Rey,[†] Jordi Rius,[‡] German Sastre,[†] and José A. Vidal-Moya[†]

Instituto de Tecnología Química, UPV-CSIC, Universidad Politécnica de Valencia, Avda. de los Naranjos s/n, 46022 Valencia, Spain, and Institut de Ciència de Materials de Barcelona (CSIC), Campus de la UAB, 08193 Bellaterra, Catalunya, Spain

Received April 7, 2004; E-mail: acorma@itq.upv.es

Abstract: ITQ-21 has been synthesized in a wide range of compositions. By rationally modifying the synthesis variables and zeolite composition, it is possible to fine-tune the crystallite size from nanocrystals (<80 nm) up to microns and to avoid the competition of other phases such as CIT-5, SSZ-24, or a laminar phase that can also be synthesized with the same organic structure directing agent. By means of XRD and ^{19}F MAS NMR, Ge and Si have been localized among the different crystallographic positions, and it is shown that Ge preferentially occupies T1 positions at the D4R cages, avoiding formation of Ge−O−Ge pairs. However, at high Ge loadings (Si/Ge = 1.7), a new ^{19}F MAS NMR signal at −14 ppm has been observed and assigned to the presence of Ge−O−Ge in Ge-rich D4R cages. Energetic configurations obtained by theoretical calculations fully agree with experimental observations, with the following increasing order in energy for Ge substitution: T1 < T2 < Ge−O−Ge in T1 < T3.

Introduction

Microporous crystalline solids, and particularly zeolites, are being extensively used for gas adsorption and separation, as ion exchangers, and for the preparation of solid catalysts.[1] Recently, the possibilities of these materials have been expanded to the fields of electronics, optics, and medicine.[2] For many of the above zeolite applications, it would be highly desirable to possess materials with large void volumes accessible through large-pore windows with the lowest diffusional limitations. This can be achieved by increasing the connectivity and pore opening of the channels that form the zeolite structure. Therefore, fully interconnected three-dimensional large-pore (12 member rings (MR)) or ultra-large-pore (>12 MR) zeolites are the most desired structures for those applications.

Up to the recent discovery of ITQ-21,[3] only four zeolites were described possessing a tridirectional large pore system: Beta, which is an intergrowth of at least two closely related polymorphs,[4,5] ITQ-7,[6,7] ITQ-17,[8−10] and finally faujasite.[11] So far, the last material is the one that has found a major range of commercial applications. However, this zeolite is synthesized with a low Si/Al ratio, and postsynthesis dealumination treatments are required for most applications. On the other hand, ultra-large-pore silica-based zeolites, with pore openings larger than 12 member rings, have only been obtained, up to now, with monodirectional channels,[12−15] this limiting the number of applications.

Very recently, a new zeolite named ITQ-21, containing Si, Ge, and optionally Al as framework cations, has been reported.[3] This material presents a unique pore topology formed by nearly spherical large cavities of 1.18 nm diameter joined to six other neighboring cavities by circular 12-ring pore windows with an aperture of 0.74 nm, which results in a three-directional channel system of fully interconnected large cavities. The zeolite was synthesized by following a 2-fold structure-directing effect: on one hand, a large and rigid structure-directing organic cation, *N*(16)-methylsparteinium, to fill the pores[12,16] and, on the other hand, the directing effect of Ge toward the formation of

* To whom correspondence should be addressed. Tel: 34(96)3877800. Fax: 34(96)3877809.
[†] Universidad Politécnica de Valencia.
[‡] Campus de la UAB.

(1) Corma, A. *J. Catal.* **2003**, *216*, 298−312.
(2) Davis, M. E. *Nature* **2002**, *417*, 813−821.
(3) Corma, A.; Díaz-Cabañas, M. J.; Martínez-Triguero, J.; Rey, F.; Rius, J. *Nature* **2002**, *417*, 514−517.
(4) Newsam, J. M.; Treacy, M. M. J.; Koetsier, W. T.; de Gruyter, C. B. *Proc. R. Soc. London, Ser. A* **1988**, *420*, 375−405.
(5) Higgins, J. B.; LaPierre, R. B.; Schlenker, J. L.; Rohrman, A. C.; Wood, J. D.; Kerr, G. T.; Rohrbaugh, W. J. *Zeolites* **1988**, *8*, 446−452.
(6) Villaescusa, L. A.; Barret, P. A.; Camblor, M. A. *Angew. Chem., Int. Ed.* **1999**, *38*, 1997−2000.
(7) Blasco, T.; Corma, A.; Díaz-Cabañas, M. J.; Rey, F.; Vidal-Moya, J. A.; Zicovich-Wilson, *C. J. Phys. Chem. B* **2002**, *106*, 2634−3642.
(8) Conradsson, T.; Dadachov, M. S.; Zou, X. D. *Microporous Mesoporous Mater.* **2000**, *41*, 183−191.
(9) Corma, A.; Navarro, M. T.; Rey, F.; Rius, J.; Valencia, S. *Angew. Chem., Int. Ed.* **2001**, *40*, 2277−2280.
(10) Sastre, G.; Vidal-Moya, J. A.; Blasco, T.; Rius, J.; Jorda, J. L.; Navarro, M. T.; Rey, F.; Corma, A. *Angew. Chem., Int. Ed.* **2002**, *41*, 4722−4726.
(11) Bergerhoff, G.; Baur, W. H.; Nowacki, W. *N. Jb. Miner. Mh.* **1958**, 193−200.
(12) Freyhardt, C. C.; Tsapatsis, M.; Lobo, R. F.; Balkus, K. J., Jr.; Davis, M. E. *Nature* **1996**, *381*, 295−298.
(13) Wagner, P.; Yoshikawa, M.; Lovallo, M.; Tsuji, K.; Taspatsis, M.; Davis, M. E. *Chem. Commun.* **1997**, 2179−2180.
(14) Burton, A.; Elomari, S.; Chen, C. Y.; Medrud, R. C.; Chan, I. Y.; Bull, L. M.; Kibby, C.; Harris, T. V.; Zones, S. I.; Vittoratos, E. S. *Chem. Eur. J.* **2003**, *9*, 5737−5748.
(15) Strohmaier, K. G.; Vaughan, D. E. W. *J. Am. Chem. Soc.* **2003**, *125*, 16035−16039.
(16) Bialek, R.; Meier, W. M.; Davis, M. E.; Annen, M. *J. Zeolites* **1991**, *11*, 438−442.

10.1021/ja047990z CCC: $27.50

structures containing double 4-rings as secondary building units.[3,7,9,10,17−21] The combination of these two approaches resulted in the formation of the ITQ-21 zeolite structure.

We present here the different parameters that control the synthesis and stability of ITQ-21 zeolite and rationalize the results. We also give a detailed characterization study of this zeolite by combining X-ray diffraction techniques (XRD), multinuclear solid-state nuclear magnetic resonance spectroscopy (MAS NMR), and computational chemistry methods. In this work, the structure of the material has been further refined, while it is found how the Ge atom population varies among the different T positions in samples with different chemical compositions.

Energy minimization calculations have been performed by computer simulations, predicting the preferred T positions for Si and Ge.

Experimental Section

Synthesis. The synthesis of ITQ-21 was carried out using *N*(16)-methylsparteinium hydroxide ($C_{16}H_{29}N_2OH$) as organic structure-directing agent either in the absence[20] or in the presence of fluoride ions[3] (i.e. OH^- or F^- media, respectively).

Syntheses of ITQ-21 in fluoride media were carried out under hydrothermal conditions in Teflon-lined stainless steel autoclaves from gels of composition

$$x\mathrm{GeO_2}:(1-x)\mathrm{SiO_2}:y\mathrm{Al_2O_3}:0.50\mathrm{C_{16}H_{29}N_2OH}:0.50\mathrm{HF}:w\mathrm{H_2O}$$

In these syntheses, germanium oxide (from Aldrich) was first dissolved in the *N*(16)-methylsparteinium hydroxide solution. Tetraethyl orthosilicate and (when required) aluminum isopropoxide (both from Aldrich) were used as silica and alumina sources, respectively. They were added, and the mixture was stirred at room temperature until the Si and Al precursors were completely hydrolyzed and the gel concentration was reached. Finally, the appropriate amount of HF was added and the mixture was homogenized by mechanical stirring and autoclaved at the desired temperature under continuous rotation (30 rpm). The final solid was recovered by filtration, washed with distilled water, and dried at 373 K. The usual crystallization temperature was 448 K, but the material can be obtained even in the 408−473 K range and either in static or under tumbling conditions.

The different gel compositions used in this study to obtain Ge and Al ITQ-21 samples are reported in Tables 1 and 2, respectively. In addition to this, ITQ-21 zeolite was synthesized in fluoride-free gels with the following general molar composition:

$$x\mathrm{GeO_2}:(1-x)\mathrm{SiO_2}:y\mathrm{Al_2O_3}:0.50\mathrm{C_{16}H_{29}N_2OH}:w\mathrm{H_2O}$$

by the same procedure as that described above. The gel compositions are given in Tables 1 and 2. Samples were named as a numeral followed by F or OH, depending on whether the synthesis was carried out in fluoride or alkaline media, respectively. The chemical compositions of the ITQ-21 samples studied in this work are listed in Table 3.

Structural Characterization. (i) X-ray Diffraction. Phase identification and crystallinity determination were performed with a Philips X'Pert diffractometer using the Cu Kα radiation provided with a graphite secondary monochromator and an automatic divergence slit fixed at 10 mm of irradiation. The diffraction data were collected at 0.04 °/step and 2 s/step between 2 and 60°.

Detailed XRD analyses including Rietveld refinements were carried out on four ITQ-21 samples.

(a) The as-synthesized ITQ-21 material (sample 1.7F-ITQ-21) was obtained as described in ref 3 using F^- as the mineralizing agent (refined Si/Ge ratio ∼1.40). This XRD pattern was measured at the synchrotron line DW22 at LURE (Orsay, France). ($\lambda = 0.9611(1)$ Å; 2θ range 2.00−45.00°; counting time 3 s; step size 0.01° 2θ; sample mounted in a capillary of 1 mm diameter). The Rietveld refinement with LSP7[22] was performed with space group $Fm\bar{3}c$ using a 2θ range from 3.00 to 43.00°. Number of contributing reflections: 237. Number of geometric

Table 1. Synthesis Conditions Employed for Ge-Containing ITQ-21 Samples[a]

Si/Ge	$H_2O/(Si+Ge)$	time (days)	phase
1	3	2	ITQ-21
	20	2	ITQ-21
2	3	2	ITQ-21
	40	4	ITQ-21
5	3	2	ITQ-21
	7.5	4	ITQ-21 + CIT-5
10	3	2	ITQ-21
	7.5	6	ITQ-21 + CIT-5
20	3	5	ITQ-21
	7.5	11	ITQ-21 + CIT-5
25	3	5	ITQ-21
50	3	12	ITQ-21 + amorphous
0	3	5	SSZ-24
	7.5	5	SSZ-24
	15	5	CIT-5
1[b]	4	12	ITQ-21
2[b]	4	12	ITQ-21
5[b]	6	13	ITQ-21 + amorphous

[a] Temperature of crystallization 448 K. [b] ITQ-21 samples synthesized in fluoride-free media.

Table 2. Synthesis Conditions Employed for Al-Containing Ge-ITQ-21 Samples[a]

Si/Ge	(Si + Ge)/Al	time (days)	phase
10	25	2	ITQ-21
	50	2	ITQ-21
20	20	2	ITQ-21
	50	2	ITQ-21
20[b]	50	4	ITQ-21 + amph[c]
	50	9	ITQ-21
25	10	2	ITQ-21 + lam[d]
	25	2	ITQ-21
50	25	3	ITQ-21 + lam[d]
	50	4	ITQ-21 + lam[d]

[a] Temperature of crystallization 448 K and water/SiO_2 = 3. [b] Water/SiO_2 = 7.5. [c] anph = amorphous material. [d] lam = means lamellar phase.

Table 3. Chemical Compositions of the Most Representative Ge-ITQ-21 Samples Employed in This Work

	composition (wt %)						residue		unit cell content	
sample	N	C	H	F	Ge	Al	TG	C/N	SDA[a]	F
1.7F	2.04	14.51	2.41	1.01	27.93	0	79.89	8.3	20.7	15.5
4.4F	2.23	15.85	2.45	1.37	15.36	0	78.05	8.3	19.8	18.2
8.5F	2.47	17.48	2.76	1.75	8.67	0	73.84	8.2	23.0	23.3
14.8F	2.49	17.14	2.68	1.65	5.26	0	73.89	8.0	21.9	21.3
14.6FAl	2.40	17.02	2.56	0.75	5.42	1.26	74.28	8.2	21.6	9.6
1.8OH	2.18	15.32	2.32	0	27.37	0	79.770	8.2	21.4	0

[a] SDA content was calculated for the C percentage.

(17) Corma, A.; Rey, F.; Valencia, S.; Jorda, J. L.; Rius, J. *Nature Mater.* **2003**, *2*, 493−497.
(18) Castañeda, R.; Corma, A.; Fornes, V.; Rey, F.; Rius,J. *J. Am. Chem. Soc.* **2003**, *125*, 7820−7821.
(19) Vidal-Moya, J. A.; Blasco, T.; Rey, F.; Corma, A.; Puche, M. *Chem. Mater.* **2003**, *15*, 3961−3963.
(20) Corma, A.; Díaz Cabañas, M. J.; Rey, F. *Chem. Commun.* **2003**, 1050−1051.
(21) Corma, A.; Navarro, M. T.; Rey, F.; Valencia, S. *Chem. Commun.* **2001**, 1486−1487.
(22) Rius, J. LSP7 Program: A Program for Restrained Rietveld Refinement; Instituto de Ciencia de Materiales de Barcelona, CSIC, Barcelona, Spain.

Table 4. Fractional Atomic Coordinates[a,b] for Calcined ITQ-21 (Si/Ge = 1.40)

atom	*x*	*y*	*z*	occ	no. of sites, Wyckoff notation
T1[c]	0.1146(7)	*x*	0.3923(6)	1	24, m
T2[c]	0.2014(7)	*x*	*x*	1	8, g
T3[c]	0.1165(7)	*x*	0	0.911 · $^1/_3$	12, i
O1	0	0.1369(20)	0.3626(16)	1	24, k
O2	0.1509(28)	*x*	$^1/_2$	1	12, j
O3	0.18293(15)	*x*	0.3194(8)	1	24, m
O4	0.1471(27)	*x*	0.1093(10)	$^1/_3$	24, m
O5	0	0.1321(29)	0	0.911 · $^2/_3$	6, e

[a] As obtained from Rietveld refinement (space group $Pm\bar{3}m$: a =13.691(2) Å). [b] Estimated standard deviations given in parentheses. [c] Atomic occupations for T sites and O5 fixed according to previous values from Rietveld refinement with synchrotron data of as-prepared ITQ-21 (see Table S1 in the Supporting Information).

Table 5. Distribution of the Ge and Si Contents along the Different T Sites of ITQ-21 for Two Different Si/Ge Ratios, As Obtained from the Rietveld Refinement of Patterns of Samples 1.7F-ITQ-21 (1.41) and 4.4F-ITQ-21 (5.15)

exptl	site T1		site T2		site T3		refined
Si/Ge	Ge	Si	Ge	Si	Ge	Si	Si/Ge[a]
1.7	0.49(1)	0.51	0.40(1)	0.60		0.91(3)	1.41
4.4	0.24(1)	0.76		0.96(2)		0.94(3)	5.15

[a] Assuming that all T sites are filled.

restraints: type d(T−O) = 1.68(2)−1.62(2) Å, 12×; type d(O−T−O) = 2.76(12)−2.65(12) Å, 18×. Number of structural parameters: 25. Number of profile parameters: 8, including unit cell parameters and zero shift (a = 27.966(1) Å, $\Delta 2\theta$ = −0.0048° 2θ) with visually estimated backgrounds. The profile function was Pearson-VII. Refined overall thermal coefficient: B = 3.2(3) Å^2. The residuals of the refinement were R_{wp} = 0.091, R_p = 0.070, and R_B = 0.042. The final atomic coordinates are given as Supporting Information in Table S1. Relevant to the present study are the refined atomic compositions at the T sites: T1, 0.51(1) Si + 0.49(1) Ge; T2, 0.60(1) Si + 0.40(1) Ge; T3, 0.91(3)Si.

(b) The same material (1.7F-ITQ-21 sample) after calcination at 500 °C in air for 2 h was obtained. The sample was cooled, and the pattern was measured at room temperature under vacuum within an Anton Paar HTK-16 high-temperature chamber attached to a diffractometer (Phillips X'Pert) with Bragg−Brentano geometry using a Pt sample holder and graphite secondary monochromator. Intensity data were obtained with a variable divergence slit. Cu K$\alpha_{1,2}$ radiation was used (λ = 1.5406, 1.5444 Å). Tube voltage and intensity: 45 kV and 40 mA. Step scan size and time: 0.02° 2θ and 13.5 s, respectively. The Cu Kα_2 contribution was mathematically stripped. The transmission coefficient at the Pt(111) Bragg position is 0.90, which is used for correcting the finite thickness of the sample. The Rietveld refinement with LSP7 was performed with space group $Pm\bar{3}m$ using a 2θ range from 5.00 to 39.00° due to the rapid falloff of the diffracted intensities. Number of contributing reflections: 39. Number of geometric restraints: type d(T−O) = 1.68(2)−1.62(2) Å, 12×; type d(O−T−O) = 2.74(12) Å, 18×. Number of structural parameters: 13, with all occupancies fixed according to the values obtained with the pattern of the as-made 1.7F-ITQ-21 sample. Number of profile parameters: 6, including unit cell parameters and zero shift (0.065° 2θ) with visually estimated background. The profile function was Pearson-VII. The refined overall thermal coefficient is B = 35(1) Å^2, which reflects the rapid decay of the diffraction peaks in the pattern. The residuals of the refinement were R_{wp} = 0.073, R_p = 0.059, and R_b = 0.077. The final atomic coordinates are given in Table 4. The refined atomic compositions at the T sites are given in Table 5.

(c) The sample 1.8OH-ITQ-21 was synthesized in OH^- media and calcined. The treatment of the material and the measurement conditions of this pattern are similar to those used for obtaining the pattern of the calcined 1.7F-ITQ-21 sample. As we will discuss later, this pattern was only used for determining the space group of calcined ITQ-21.

(d) The as-synthesized ITQ-21 material (4.4F-ITQ-21 sample) was obtained using fluoride media with an Si/Ge ratio of ∼4.5. This pattern was collected on an X'Pert diffractometer equipped with a secondary graphite monochromator. Measurement conditions: flat sample; Cu Kα_{12} radiation; automatic divergence slit (10 mm); 45 kV, 40mA; step size 0.02° 2θ; step time 40 s; 2θ interval 5−70°. The restrained Rietveld refinement with LSP7 was performed with space group $Fm\bar{3}c$. Number of contributing reflections: 223. The type and number of geometric restraints used were the same as for the Rietveld refinement of the pattern of sample 1.7F-ITQ-21 in the as-prepared form. The refinement converged to R_{wp} = 0.091, R_p = 0.070, and R_b = 0.097. The principal interest of the Rietveld refinement of this pattern is the determination of the Ge content at the different T sites. The distribution found is given in Table 5.

(ii) Solid State NMR. The NMR spectra were recorded at room temperature under magic angle spinning (MAS) in a Bruker AV-400 spectrometer. ^{19}F was measured at 376.28 MHz using a Bruker probe with 2.5 mm diameter zirconia rotors spinning at 25 kHz. The ^{19}F spectra were collected using pulses of 4.5 μs corresponding to a flip angle of $\Pi/2$ rad, and a recycle delay of 100 s to ensure the complete recovery of the magnetization. The single pulse ^{29}Si spectra were acquired at 79.5 MHz with a 7 mm Bruker BL-7 probe using pulses of 3.5 μs corresponding to a flip angle of 3/4 Π radians, and a recycle delay of 240 s. The ^{19}F to ^{29}Si cross polarization (CP) spectra were measured with a Doty XC4 probe with zirconia rotors (4 mm in diameter). The ^{19}F $\Pi/2$ pulse length was 9 μs, and the contact time 5 ms. The ^{19}F and ^{29}Si spectra were referred at $CFCl_3$ and tetramethylsilane, respectively.

(iii) Computer Simulations. Force Field. The Born model with inclusion of dipolar polarization of oxygen has been used, as was done in previous works.[23] It consists of the Coulomb interaction, evaluated via an Ewald summation, a short-range pair potential described by a Buckingham function with cutoff distance of 12 Å, and a three-body angle bending term (O−Si−O). The shell model was used to simulate the polarizability of the oxygen ions. For the germanium case, the three-body bending term was omitted on the basis that 6-fold- as well as 4-fold-coordinated structures are taken into account in the fit. The functional forms are

$$E^{\text{silica}} = E^{\text{Buckingham}} + E^{\text{three-body}} + E^{\text{core-shell}} + E^{\text{Coulombic}} \quad (1)$$

$$E^{\text{germania}} = E^{\text{Buckingham}} + E^{\text{core-shell}} + E^{\text{Coulombic}} \quad (2)$$

$$E_{ij}^{\text{Buckingham}} = A_{ij}\exp\left(-\frac{r_{ij}}{\rho_{ij}}\right) - \frac{C_{ij}}{r_{ij}^6} \quad (3)$$

$$E_{ijk}^{\text{three-body}} = \frac{1}{2}k_{ijk}(\theta - \theta_0)^2 \quad (4)$$

$$E_{ij}^{\text{core-shell}} = \frac{1}{2}k_{ij}^{\text{cs}}r_{ij}^2 \quad (5)$$

$$E_{ij}^{\text{Coulombic}} = \frac{q_i q_j}{4\pi\epsilon_0 r_{ij}} \quad (6)$$

The energy expression also includes the terms of the SDA occluded in the microporous voids of the zeolite. The total potential energy function and the respective terms are

$$E^{\text{total}} = E^{\text{zeolite}} + E^{\text{SDA}} + E^{\text{zeolite-SDA}} + E^{\text{SDA-SDA}} \quad (7)$$

Table 6. Atomic Charges and Number of Atoms of Each Type for the *N*-Methylsparteinium Cation Used in the Synthesis of ITQ-21[a]

atom	charge	no. of atoms	atom	charge	no. of atoms
N4	−0.3354	1	C2	−0.1902	11
N3	−0.3284	1	C3	0.0072	4
C1	−0.2110	1	H	0.1358	29

[a] N4 and N3 are quaternary and tertiary nitrogen; C1, C2, and C3 are primary, secondary, and tertiary carbon, respectively.

The E^{zeolite} term has already been described in eqs 1−6, and the other terms are

$$E^{\text{SDA}} = E^{\text{harmonic}} + E^{\text{three-body}} + E^{\text{torsion}} + E^{\text{Coulombic}} \quad (8)$$

$$E^{\text{zeolite-SDA}} = E^{\text{Lennard-Jones}} + E^{\text{Coulombic}} \quad (9)$$

$$E^{\text{SDA-SDA}} = E^{\text{Lennard-Jones}} + E^{\text{Coulombic}} \quad (10)$$

Three-body and Coulombic terms have already been described in eqs 4 and 6, and the other terms are

$$E_{ij}^{\text{harmonic}} = \frac{1}{2}k_{ij}^{\text{h}}(r_{ij} - r_{ij}^{0})^2 \quad (11)$$

$$E_{ijkl}^{\text{torsion}} = k_{ijkl}^{\text{t}}[1 + \cos(n\phi - \phi_0)] \quad (12)$$

$$E_{ij}^{\text{Lennard-Jones}} = \frac{B_{ij}^{\text{LJ}}}{r_{ij}^{12}} - \frac{C_{ij}^{\text{LJ}}}{r_{ij}^{6}} \quad (13)$$

The force field by Kiselev et al.[24] was selected for the intermolecular SDA−zeolite and SDA−SDA interactions, for which it has been successfully used previously, while the force field by Oie et al.[25] was used to provide the remaining intramolecular interactions between the atoms of the organic—a task to which it is well suited, having been designed to reproduce a wide range of organic crystal structures. The SDA used in the synthesis of Ge-ITQ-21 is the *N*(16)-methylsparteinium cation, and in order to treat in a realistic way the electrostatics of the interaction between the SDA and the zeolite, and between organic molecules, previous full optimizations of the charged templates have been carried out at the ab initio Hartree−Fock level with the 6-31G** basis set, using the program NWChem.[26] The corresponding charges are listed in Table 6. Finally, the positive charge introduced by the presence of the organic is compensated by inclusion of fluoride anions, thus resembling the final zeolite composition. The force field by George and Catlow[27] has been used to treat the interaction of fluoride with the zeolite.

All the optimizations in this work have been carried out with SDA filling the micropore. This effect has been shown to influence the energetics of the final system and the heteroatom distribution observed.[28−30] The GULP implementation of this methodology has been used throughout.[31]

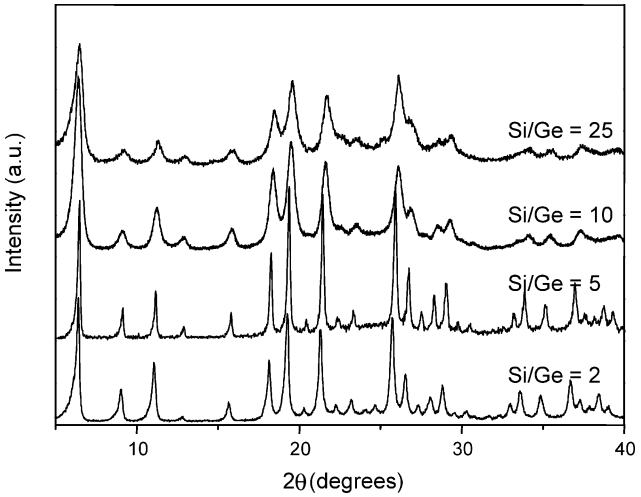

Figure 1. X-ray diffraction patterns of representative as-synthesized zeolites ITQ-21 with different Ge contents.

Results and Discussion

Synthesis. *N*(16)-Methylsparteinium (MSPT) cation has been previously used as an effective SDA for crystallization of CIT-5[12,13] and SSZ-24[16] (IZA codes: CFI and AFI, respectively), which are high-silica zeolites with a one-dimensional channel system. With *N*(16)-methylsparteinium as structure-directing agent and introduction of Ge in the synthesis gel, it is possible to obtain ITQ-21 within a large interval of chemical compositions. Indeed, the results given in Table 1 show that Al-free ITQ-21 zeolite can be prepared with a Si/Ge ratio of between 2 and 50 using the synthesis conditions assayed here. It has to be pointed out that the crystallization rate of ITQ-21 is accelerated as the Ge content in the synthesis gel increases.

A deeper understanding of the crystallization kinetics of Ge-containing ITQ-21 zeolites can be obtained by inspecting the crystallization curves of ITQ-21 samples synthesized by varying the Ge content in the initial reaction mixture (Figure S1, given as Supporting Information). Fully crystalline materials are obtained from synthesis gels with Si/Ge = 5 in only 6 h, whereas a crystallinity of only 30% was reached after 6 h when the Si/Ge ratio in the synthesis gels was 15 and 100% after 48 h. When the Si/Ge ratio of the synthesis gel is increased to 25, 4 days was required to achieve 100% of crystallinity, under the synthesis conditions reported here. Representative XRD patterns of ITQ-21 samples with different Si/Ge ratios are given in Figure 1.

One of the most striking features of these crystallization curves is that no induction period was observed at measurable times. This clearly suggests that nucleation occurs very fast, indicating a high stability of the nuclei formed under the synthesis conditions employed here. It is worth noting that the second step on the crystallization curves, i.e., crystal growth, strongly depends on Ge concentration. Then, when the Ge content is increased, the slope of the crystallization curve, related to the formation of crystals from the nuclei, strongly increases. These results can be explained by considering that highly stable Ge-enriched nuclei are formed at the earliest stage of crystallization (nucleation), which immediately start to grow to form ITQ-21 zeolite. Then, a strong dependence between nuclei

(23) Sastre, G.; Leiva, S.; Sabater, M. J.; Giménez, I.; Rey, F.; Valencia, S.; Corma, A. *J. Phys. Chem. B* **2003**, *107*, 5432−5440.
(24) Kiselev, A. V.; Lopatkin, A. A.; Shul'ga, A. A. *Zeolites* **1985**, *5*, 261−267.
(25) Oie, T.; Maggiora, T. M.; Christoffersen, R. E.; Duchamp, D. J. *Int. J. Quantum Chem., Quantum Biol. Symp.* **1981**, *8*, 1−47.
(26) Harrison, R.; Nichols, J.; Straatsma, T.; Dupuis, M.; Bylaska, E.; Fann, G.; Windus, T.; Apra, E.; Anchell, J.; Bernholdt, D.; Borowski, P.; Clark, T.; Clerc, D.; Dachsel, H.; de Jong, B.; Deegan, M.; Dyall, K.; Elwood, D.; Fruchtl, H.; Glendenning, E.; Gutowski, M.; Hess, A.; Jaffe, J.; Johnson, B.; Ju, J.; Kendall, R.; Kobayash, R.; Kutteh, R.; Lin, Z.; Littlefield, R.; Long, X.; Meng, B.; Nieplocha, J.; Niu, S.; Rosing, M.; Sandrone, G.; Stave, M.; Taylor, H.; Thomas, G.; van Lenthe, J.; Wolinski, K.; Wong, A.; Zhang, Z. NWChem, A Computational Chemistry Package for Parallel Computers, Version 4.0; Pacific Northwest National Laboratory, Richland, WA 99352-0999, 2000.
(27) George, A. R.; Catlow, C. R. A. *Zeolites* **1997**, *18*, 67−70.
(28) Shantz, D. F.; Fild, C.; Koller, H.; Lobo, R. F. *J. Phys. Chem. B* **1999**, *103*, 10858−10865.
(29) Sabater, M. J.; Sastre, G. *Chem. Mater.* **2001**, *13*, 4520−4526.
(30) Sastre, G.; Fornes, V.; Corma, A. *J. Phys. Chem. B* **2002**, *106*, 701−708.
(31) Gale, J. D. *J. Chem. Soc., Faraday Trans.* **1997**, *93*, 629−637.

concentration and Ge content in the gel must exist, and relatively low Ge concentrations will result in a low concentration of "viable" nuclei and, consequently, in a reduction of the crystallization rate.

It could be concluded that the presence of Ge in the synthesis gel clearly favors the nucleation and crystallization of ITQ-21 zeolite. This finding has been attributed to the strong stabilization effect of Ge when located in D4R units, present in ITQ-21. This hypothesis is also supported by the fact that CIT-5 and SSZ-24, which do not contain such D4R units in their structures, strongly compete when the synthesis is carried out in the absence of Ge.

The $H_2O/(Si + Ge)$ ratio plays an important role in the synthesis of Ge-ITQ-21. Indeed, high Si/Ge ratio ITQ-21 zeolites are preferentially formed in highly concentrated gels ($H_2O/(Si + Ge) \leq 3$), whereas CIT-5 or SSZ-24 starts to compete in more dilute synthesis media (see Table 1). The influence of the $H_2O/(Si + Ge)$ ratio becomes less important for low Si/Ge ratio samples, for which the most determinant synthesis parameter is the presence of Ge, which drives the crystallization toward the D4R-containing ITQ-21 zeolite structure, even when the synthesis is carried out at higher H_2O/T^{IV} ratios.

An important issue for pursuing catalytic applications is the possibility of incorporating trivalent cations in framework positions that will lead to acid properties in the final solid. As is shown in Table 2, Al-ITQ-21 is obtained in a range of Si/Ge ratios very similar to those required to prepare T^{III}-free samples. When Al is present in the synthesis gel and the amount of Ge is very low, the competing phase is neither CIT-5 nor SSZ-24 zeolite but a lamellar phase.

Finally, it is worth mentioning that it is possible to fine-tune the crystal size of ITQ-21 materials by controlling the $H_2O/(Si + Ge)$ ratio in the synthesis gel. Typically ITQ-21 zeolite grows as nanocrystalline materials (<80 nm). However, the crystal size of the resulting ITQ-21 zeolites increases when the gel concentration decreases, as is shown in Figure S2 (given as Supporting Information), where the SEM images of ITQ-21 zeolites obtained from synthesis gels of different $H_2O/(Si + Ge)$ ratios are presented.

Zeolite Stability. X-ray diffraction patterns of representative as-synthesized ITQ-21 samples with different Ge contents are shown in Figure 1. There is a progressive shift of the X-ray peaks toward higher d spaces with increasing Ge content, due to the unit cell expansion caused by the larger ionic radii of Ge with respect to Si.

"In situ" high-temperature X-ray diffraction studies show that ITQ-21 is stable at temperatures above 600 °C (Figure S3, given as Supporting Information). For instance, samples with a Si/Ge ratio equal or greater than 10 are stable at the highest temperature essayed in this work (800 °C). Moreover, the thermal stability of Ge-ITQ-21 does not depend exclusively on the Si/Ge ratio. Calcination of samples with high Ge content synthesized in OH^- media leads to highly ordered structures, whereas the analogous samples synthesized in fluoride media give broad X-ray diffraction peaks, suggesting that the latest samples possess a higher number of structural defects. This may be due to the partial destruction of some D4R cages during calcination, which could occur during the evacuation of the occluded F^-.

Table 7. Textural Properties of ITQ-21 Samples

zeolite composition		micropore	BET surface	external surface
Si/Ge	T^{IV}/T^{III}	vol (cm^3/TO_2)	($m^2\ g^{-1}$)	($m^2\ g^{-1}$)
1.7	∞	14.98	462	56
4.4	∞	14.85	541	86
8.5	∞	15.39	777	284
14.8	∞	14.46	798	310
14.6	25	14.46[a]	797[a]	301[a]
14.6	25	11.32[b]	590[b]	200[b]

[a] Sample exposed for 30 days to the atmospheric moisture. [b] Sample calcined at 550 °C and steamed at 720 °C, 3 h, 100% humidity.

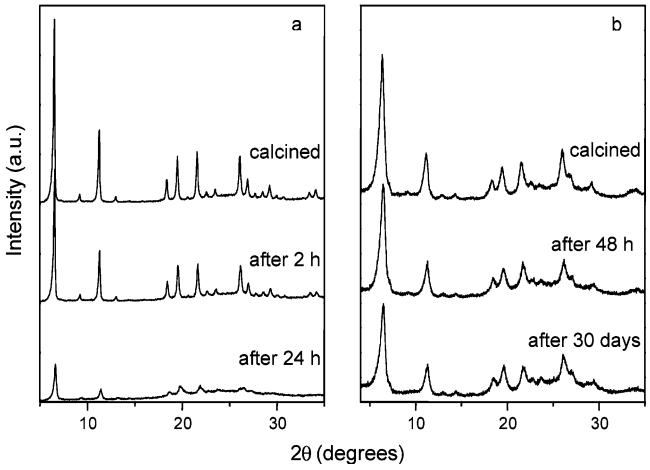

Figure 2. XRD patterns of calcined ITQ-21 samples exposed to the atmosphere: (a) 1.7F−ITQ-21 sample; (b) 14.8F-ITQ-21 sample.

The thermal stability of the ITQ-21 zeolite is also demonstrated by the nearly constant micropore volume of the samples upon calcination (Table 7). It can also be seen in Table 7 that the external surface area of the ITQ-21 samples increases as the Ge content diminishes. This observation is self-consistent with the increase of the crystal size of the samples with Ge loading.

The most important concern regarding the stability of Ge-rich ITQ-21 was that calcined samples could suffer framework damage upon exposure to the atmospheric moisture. The XRD patterns of calcined ITQ-21 samples exposed to the atmosphere for certain periods of time show (Figure 2) that the sample with the highest Ge content (Si/Ge = 2) decomposes rapidly upon exposure to the atmospheric moisture and, in contrast, the sample with the lowest Ge content (Si/Ge = 15) is stable upon prolonged exposure to wet air. In the case of Al-containing ITQ-21, the calcined samples are also stable in contact with the atmospheric moisture, and no loss of crystallinity or micropore volume (Table 7) was observed. Even more important, the zeolite retains more than 75% of the initial microporosity after steam calcination at 720 °C and 100% steam (Table 7).

Structure Refinement and Atom Location by X-ray Diffraction. The laboratory powder diffraction pattern of the as-synthesized ITQ-21 zeolite was successfully refined in space group $Fm\bar{3}c$.[3] This earlier result has been confirmed by using synchrotron XRD data. This new refinement clearly indicates that the face centering is due to the slight rotation of the D4R cages by approximately 9.6°, as shown in Figure 3 (the corresponding atomic coordinates are given as Supporting Information in Table S1). With regard to our earlier communication,[3] there are only small deviations in the values of

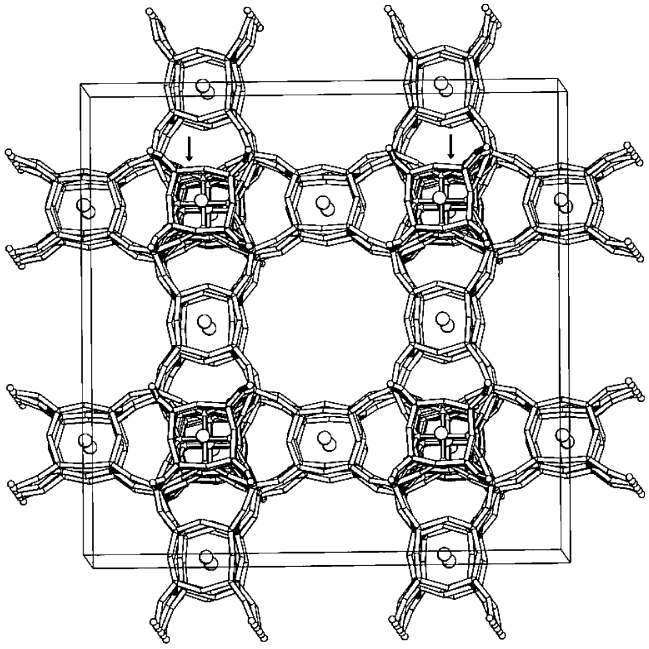

Figure 3. Perspective view of as-synthesized ITQ-21 showing the slightly rotated D4R units (arrows) and the F^- anions placed in the middle of them. For clarity the SDA has been omitted. The cubic unit cell parameter is 21.713 Å long.

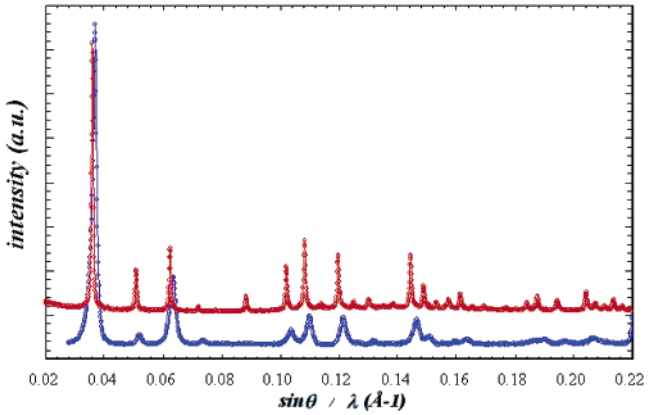

Figure 4. Powder diffraction patterns of as-synthesized (top) and calcined (bottom) 1.7F-ITQ-21. Represented 2θ interval: 5−39°. The top pattern was measured with synchrotron radiation ($\lambda = 0.9611$ Å) and the bottom one with laboratory radiation (Cu $K\alpha_1$).

the atomic coordinates and the occupancies remain practically unchanged (see Table 5).

The study of calcined ITQ-21 zeolites has been performed on samples prepared in both fluoride and alkaline media. Since ITQ-21 samples prepared in the presence of fluoride anions give materials (Figure 4) more disordered than those synthesized in alkaline media after calcination, it would be preferable to carry out the XRD study on ITQ-21 zeolites prepared under basic conditions. Unfortunately, these materials crystallize with a very small but variable amount of an unknown impurity (marked as *i* in the bottom pattern of Figure 5), which allows the space group determination but prevents using their data for accurate Rietveld refinement studies. Figure 5 compares the pattern of the as-synthesized 1.7F-ITQ-21 sample to the pattern of calcined 1.8OH-ITQ-21 material. There, it can be clearly seen that the weak superstructure peaks due to the face centering (marked as *F* in Figure 5) are no longer present in the calcined sample,

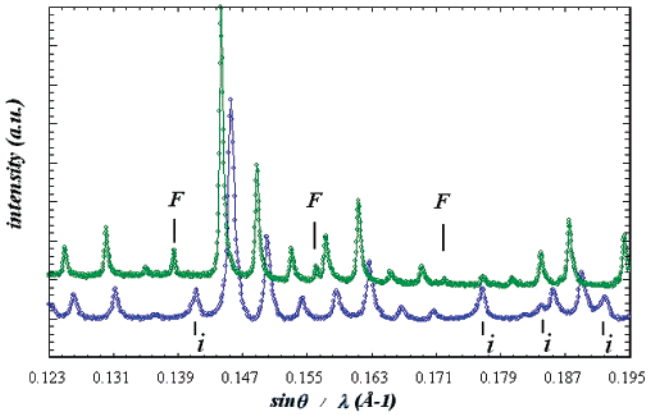

Figure 5. Comparison of two portions of the powder patterns of the as-synthesized 1.7F-ITQ-21 (top) and calcined 1.8OH-ITQ-21 (bottom) samples. In the top pattern, the symbol *F* denotes the weak superstructure reflections due to the face centering, not present in the bottom pattern. The bottom pattern corresponds to a material obtained in a basic medium (i.e without F^- anions), which shows good crystallinity after calcination. Unfortunately, this pattern includes peaks from an unknown impurity (denoted as *i* in the bottom pattern), which when resolved can be easily distinguished by its different asymmetry.

thus indicating a primitive cubic unit cell. Since, in addition, no systematic extinctions are observed, the most probable centrosymmetrical space group for the structure of the calcined ITQ-21 material is $Pm\bar{3}m$ (No. 221), instead of space group $Fm\bar{3}c$ found for the as-synthesized ITQ-21 material. Accordingly, the Rietveld refinement of the calcined ITQ-21 material (with F^- as mineralizing agent) was performed with this space group. Figure S4 (given as Supporting Information) reproduces the observed and calculated powder diffraction patterns. To compensate for the loss of information due to the broadening of the diffraction peaks, the cationic compositions of the T sites were introduced as additional observations in the refinement. These were previously derived from the Rietveld refinement with synchrotron data of the corresponding as-synthesized sample by assuming, as has been already confirmed for other Ge-containing zeolites, that no significant Ge lattice mobility occurs during calcination.[10] The somewhat too low refined occupancies of T3 (Si) and O5, i.e., 0.91(3), could indicate a small amount of basic units without inner four-membered rings. The final atomic coordinates for the calcined sample are listed in Table 4, with the atom numbering given in Figure 6.

For clarity, only O4, T3, and O5 atomic positions corresponding to one orientation of the inner four-membered ring are depicted in this figure. The observed enrichment of Ge at sites T1 and T2, shown in Table 5, is further supported by the enlargement of the corresponding T1−O and T2−O distances, as expected from the larger ionic radius of Ge when compared to Si (see Table S2 of the Supporting Information). Also, it is even more notorious that T3 remains as nearly pure siliceous even in a sample having a Si/Ge ratio of 1.7 (Table 5), indicating that this particular site is highly disadvantaged for Ge occupation.

Additionally, the averaged T1−O−T angles are narrower (between 129 and 144°) than T3−O−T angles (162−165°), indicating that the presence of Ge allows reduction of the typical T−O−T angle for purely siliceous materials and, therefore, favors the formation of strained D4R cages (see Table S2 of the Supporting Information).

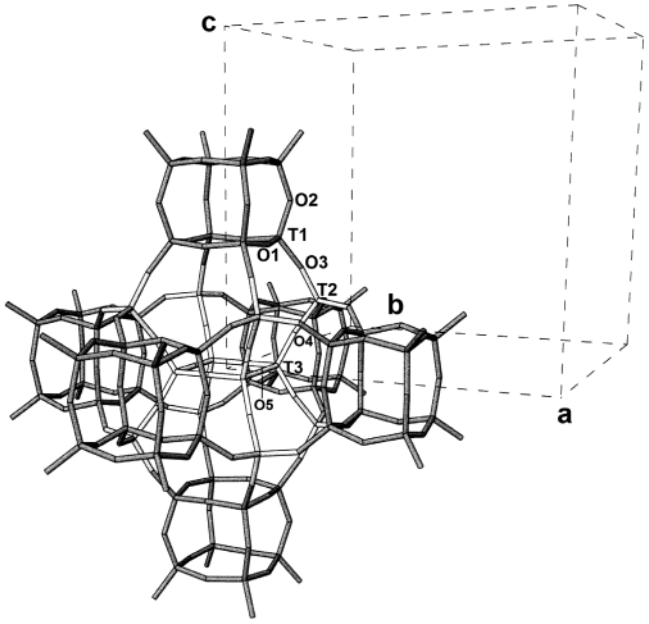

Figure 6. Perspective view of the basic unit of calcined ITQ-21 corresponding to the $Pm\bar{3}m$ space group symmetry ($a = 13.69$ Å). For clarity, only the O4, T3, and O5 atomic positions corresponding to one orientation of the inner 4-ring are depicted.

The preferential occupation of T1 sites by Ge atoms is better demonstrated by the results obtained for ITQ-21 zeolites with a higher Si/Ge ratio in their compositions. In Table 5, the refined T site occupations for samples with Si/Ge ratios of 1.7 and 4.5 are shown. It can be clearly seen that, for low Ge content, this tends to be placed at the T1 sites, while T2 and T3 positions remain as pure or nearly pure siliceous. When the Ge content increases, T2 sites are also occupied by Ge atoms, but T3 sites do not accept any Ge. These results clearly speak for the different relative energies of Ge placed at the various T sites of the ITQ-21 structure, and this will be the subject of energy calculations using computer simulations in the last part of the paper.

MAS NMR Characterization. We have previously shown for other Ge zeolites with D4R that F^- is located in these small cages and they can act as an NMR probe, giving information on the distribution of Ge atoms among the cages.[7,10,19]

The ^{19}F MAS NMR spectra of ITQ-21 zeolites with different Si/Ge ratios are shown in Figure 7. The spectrum of the sample with a Si/Ge ratio of 8.5 consists of three peaks at −38, −20, and −8 ppm, which were previously observed in the other Ge zeolites having D4R cages in their structures and assigned to fluoride anions in cages with (8Si, 0Ge), (7Si, 1Ge), and (5Si, 3Ge) or (4Si, 4Ge), respectively.[7,10,19,32] The relative intensity of the peak at −38 ppm and that at −20 ppm decreases when the germanium content increases and disappears for Si/Ge = 1.7, while the signal at −8 ppm increases in this range of compositions. The spectrum of the ITQ-21 sample with Si/Ge =1.7 shows a signal at −8 ppm with a shoulder at −14 ppm. This latter chemical shift is consistent with fluoride ions in D4R cages containing more than 4 Ge atoms or even pure $GeO_{4/2}$.[33]

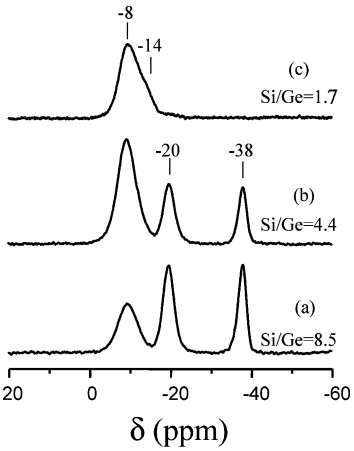

Figure 7. ^{19}F MAS NMR spectra of Ge-ITQ-21 samples with Si/Ge ratios of (a) 8.5, (b) 4.4, and (c) 1.7.

Table 8. Intensity of the ^{19}F NMR Signals Referred to 100[a]

	^{19}F				
sample	−8 ppm	−20 ppm	−38 ppm	% Ge T1	Si/Ge_{NMR}
Si/Ge = 1.7	100	0	0	38	3.0
Si/Ge = 4.4	62.5	22.5	15.0	26	4.7
Si/Ge = 8.5	32.0	37.0	31.0	15	8.3

[a] Occupancy of the T1 sites by Ge expressed in percent. This value (% Ge T1) is calculated with the formula given in ref 7 and the following assignment of the ^{19}F peaks: −38 ppm to F(8Si), −20 ppm to F(7Si,1Ge) and −8 ppm to F(5Si,3Ge). Si/Ge_{NMR} is calculated by assuming that Ge only occupies T1 sites.

Table 8 collects the relative areas of three ^{19}F NMR peaks for the Ge-containing ITQ-21. Because of the poor resolution of the component at −14 ppm in the spectrum of sample 1.7Ge-ITQ-21, along with the uncertainty in its assignment, we have ignored it in Table 8. The Ge T1 site occupancy and the $(Si/Ge)_{D4R}$ ratio were calculated by following the procedure indicated in the legend. We must note the good agreement of the Ge T1 occupancy in the 4.4Ge-ITQ-21 sample with that obtained from the XRD data, reinforcing the interpretation of the ^{19}F NMR spectra. The higher $(Si/Ge)_{D4R}$ ratio estimated from NMR data for the sample 1.7Ge-ITQ-21 comes from the presence of a signal at −14 ppm, assigned to fluoride anions located at enriched Ge D4R cages,[33] which is included within the area of the peak at −8 ppm. Again, the results clearly indicate that Ge preferentially substitutes for Si at the D4R units. For Ge-rich samples, this and the appearance of the ^{19}F signal at −14 ppm from Ge-rich cages strongly suggest that the incorporation of Ge heteroatoms at crystallographic T1 sites at the D4R units occurs to a higher extent than it does in other Ge-containing zeolites. In Ge-ITQ-7 and Ge-ITQ-17, other crystallographic sites become occupied when the Ge content is higher than that required to introduce three or four Ge atoms per D4R cage.

The ^{29}Si MAS NMR spectra of Ge-containing ITQ-21 zeolites, shown in Figure 8, consist of a weak peak at −120 ppm and a broad band with a maximum at ca. −106 ppm, resulting from the contribution of silicon atoms at different crystallographic sites and with a varying number of Ge atoms in its second coordination shell.[34] Figure S5 (given as Supporting

(32) Caullet, P.; Guth, J. L.; Hazm, J.; Lamblin, J. M.; Gies, H. *Eur. J. Solid State Inorg. Chem.* **1991**, *28*, 345−61.
(33) Wang, Y.; Song, J.; Gies, H. *Solid State Sci.* **2003**, *5*, 1421−1433.
(34) Kosslick, H.; Tuan, V. A.; Fricke, R.; Peuker, C.; Pilz, W.; Storek, W. *J. Phys. Chem.* **1993**, *97*, 5678−5684.

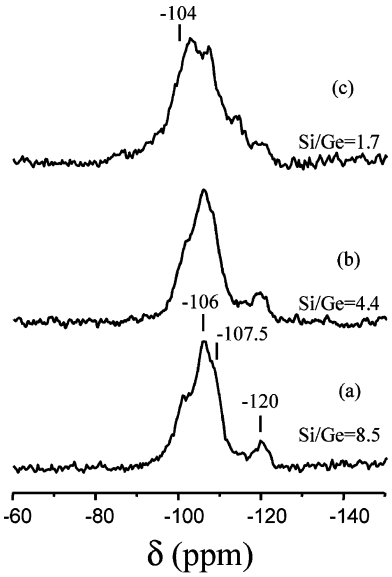

Figure 8. ^{29}Si MAS NMR spectra of Ge-ITQ-21 samples with Si/Ge ratios of (a) 8.5, (b) 4.4, and (c) 1.7.

Information) compares the ^{29}Si MAS NMR spectra of the sample with Si/Ge = 8.5 recorded with a single pulse and under ^{19}F to ^{29}Si cross-polarization (CP) conditions. The CP/MAS technique, which selectively enhances the ^{29}Si peaks of atoms in the proximity of fluoride ions, provokes the near-disappearance of the high-field peak at −120 ppm. This indicates that the signals of silicon atoms at D4R, with and without Ge in its second coordination shell, are included in the broad band. The relative intensity of the peak at −120 ppm is practically the same for the samples with Si/Ge ratios of 8.5 and 4.4, and this is only modified in the richer Ge sample (Si/Ge = 1.7). In addition to this, the chemical shift agrees well with that predicted for the T3 sites (122.1 ppm) on the basis of its average Si−O−Si bond angle (167°).[35] These observations allow us to attribute the peak at −120 ppm to Si (4Si) T3 sites of the ITQ-21 structure.

To summarize, the multinuclear NMR results also indicate the preferential incorporation of Ge at the D4R sites in the ITQ-21 structure, as was observed by means of XRD techniques. Interestingly, in Ge-rich ITQ-21 samples, the NMR results suggest the formation of Ge−O−Ge bonds, which were not observed in Ge-ITQ-7 and Ge-ITQ-17 at equivalent Ge/D4R ratios.

The nonrandom distribution of Ge in the structure of ITQ-21, and its differences with other Si−Ge zeolites, should be related with differences of energy for occupancy of the different T positions by Ge. This will be studied below by means of theoretical calculations.

Computer Simulations. The use of computer simulations can be helpful for understanding the relative stabilities of different phases through the calculation of the framework energies. In this case, preferential locations for germanium could be established by calculating the relative energies of the statistically sampled distributions over the entire compositional range of Si/Ge ratios. It is especially interesting to do that in our case, where the Ge sites have been localized by both XRD and NMR techniques. This should allow us to test if this methodology can be used to predict the atomic distribution among the different positions within the structure. It has to be said that, aside from using first-principles calculations,[7,36,37] the interatomic potential approach has also rendered valuable results[38−40] and, owing to the significantly lower computational expense, it is very adequate when a large number of possibilities have to be explored. However, to be successful as a predictive tool, it is essential to ensure that the force field is of the highest quality. A recently parametrized force field for Si/Ge zeolites[41] has taken into account a larger set of structures than was the case for previous models,[27,42] in order to maximize transferability, and it has been successfully tested in reproducing the structural features of ASU-7 and ASU-9[43] as well as Ge-ITQ-17.[10]

Here, the pure silica polymorph of ITQ-21 has been used for minimizing the unit cell of the structure. For doing this, we have chosen the *translationsgleich* subgroup *I*4/*mcm* (No. 140) of space group $Fm\bar{3}c$, so that the 4-ring (4R) located inside the [$4^6 6^{12}$] cage is not longer averaged but oriented normal to the *c* axis. This symmetry reduction increases the number of symmetry-independent T sites from three to four as a consequence of the splitting of the T1 site into T1 and T1′. For computational efficiency, the starting values were calculated from the 8× smaller unit cell of calcined ITQ-21 (a = 13.69 Å) by assuming *P*4/*mmm* symmetry. The three D4R groups present in the unit cell were filled with fluoride anions, and three MSPT cations were introduced in the microporous voids of the zeolite. A large number of orientations of the organic cations in the micropore of ITQ-21 were tested and minimized in order to find the most favorable interaction of the SDA with the zeolite walls. The cell parameters and the averaged bond distances and angles for the optimized pure silica ITQ-21 zeolite are shown as Supporting Information in Table S3. During the optimization, the fluoride anions have been kept fixed in the center of the D4R, and also the cell angles have been kept fixed to 90°. Apart from that, all the other cell parameters and the coordinates of all the atoms of the zeolite and the SDA have been allowed to relax. From the results of Table S3, the T−O distances seem to indicate that the most suitable positions for Ge would be the T sites placed at the D4R, T1 and T1′, because they have already slightly larger T−O distances (1.626 and 1.630 Å, respectively) than in the case of T2 and T3 (1.615 and 1.594 Å, respectively). The inspection of the T−O−T angles confirms this observation, since T1−O−T1, T1′−O−T1′ and T1′−O−T2, all with angles below 140°, will be more suitable for Ge−O−Si linkages.

(i) Ge-ITQ-21 with One Ge per Unit Cell. Following the previous calculation, one Ge atom has substituted for one Si and the subsequent unit cell ($GeSi_{35}O_{72}$), with the fluoride anions and the SDA molecules as in the previous case, has again been optimized. This has been done for the four different T sites, and the results are shown in Table S4 of the Supporting Information. It is seen that, in all cases, the T−O−T average

(35) Thomas, J. M.; Klinowski, J.; Ramdas, S.; Hunter, B. K.; Tennakoon, D. B. T. *Chem. Phys. Lett*. **1983**, *102*, 158−162.
(36) Jolly, L. H.; Silvi, B.; D'Arco, P. *Eur. J. Miner.* **1994**, *6*, 7−16.
(37) Christie, D. M.; Chelikowsky, J. R. *Phys. Rev. B* **2000**, *62*, 14703−14711.
(38) *Computer Simulations of Solids*; Lecture Notes in Physics 166; Catlow, C. R. A., Mackrodt, W. C., Eds., Springer-Verlag: Berlin, 1982.
(39) *Modelling of Structure and Reactivity in Zeolites*; Catlow, C. R. A., Ed., Academic Press: London, 1992.
(40) Catlow, C. R. A.; Bell, R. G.; Gale, J. D. *J. Mater. Chem.* **1994**, *4*, 781−792.
(41) Sastre, G.; Gale, J. D. *Chem. Mater.* **2003**, *15*, 1788−1796.
(42) Tsuchiya, T.; Yamanaka, T.; Matsui, M. *Phys. Chem. Miner.* **1998**, *25*, 94−100.
(43) Li, H.; Yaghi, O. M. *J. Am. Chem. Soc.* **1998**, *120*, 10569−10570.

angles decrease upon Ge incorporation as a consequence of Ge−O−Si being smaller than Si−O−Si equilibrium angles. Meanwhile, the T−O distances tend to enlarge, aiming to reach values as close to 1.74 Å as possible. T1 and T1′ sites seem to fulfill this condition, helped by the fact, as pointed above, that the T−O distances in those sites are larger before the Ge incorporation. Additionally, if the flexibility of the site allows this, then the final Ge−O distances are about 1.74 Å and some more strain is observed in T2, where only 1.727 Å can be reached after Ge incorporation. This is also reflected in the greater substitution energy for T2 (46.3 kJ/mol) with respect to T1 and T1′ sites. The large T−O−T angle observed (143.2°, Table S4) also contributes to the greater substitution energy obtained for Ge in T2 positions. Even greater substitution impediment is observed for the T3 position. In this case, final average T−O−T angles are 150.7°, and the Ge−O distance can only reach 1.708 Å with the corresponding high incorporation energy (78.4 kJ/mol). The theoretical results are in complete agreement with the preferential occupancy of Ge for positions T1/T1′ at the D4R units, observed by X-ray diffraction and ^{19}F MAS NMR studies. Thus, given the large energy difference between T1/T1′ substitution energies and the first non-D4R germanium sitting at T2, this latter position should not be appreciably populated until D4R units contain more than three or four germanium atoms. The three D4R units per unit cell correspond to 24 atoms out of a total of 36 T sites, and three or four Ge atoms per D4R give framework Si/Ge = 3 and Si/Ge = 2, respectively. Therefore, at Si/Ge > 2, Ge should be, by and large, preferentially located at T1/T1′ positions.

(ii) Ge-ITQ-21 with Si/Ge = 2. A series of simulations have been carried out with the unit cell $Ge_{12}Si_{24}O_{72}$, including also the three fluoride anions and the three *N*-methylsparteinium cations as in the previous cases. Although there are many possible distributions of Ge over the T1/T1′, T2, and T3 sites fulfilling Si/Ge = 2, only cases with Ge1 + Ge1′ = 12 have been considered, with the aim of studying the effect of Ge−Ge ordering on the total energy. Therefore, 12 Ge atoms are distributed over T1/T1′ positions, while the remaining 24 T sites (8 T2 + 4 T3 + 12 T1/T1′) are therefore occupied by Si. A computer-generated algorithm for random sampling, fulfilling all these conditions, has been automated to generate the distributions.

Apart from the considerations regarding the substitution energies, a new effect, the Ge−Ge interaction, appears here when more than one Ge atom is introduced in the framework. It is believed that Ge tends to locate as far apart as possible from each other, and this is the point that we address now with the following calculations. It is clear that, by selecting the unique configuration Ge1 + Ge1′ = 12, the energetic effect coming from *site energetics* is eliminated, due to the fact that the incorporation of Ge in T1 and T1′ gives similar values (see Table S4 in the Supporting Information). Therefore, energy differences among various configurations should be mainly ascribed to Ge−Ge interactions. Elongation of contiguous Ge−O bonds linked to a common oxygen will cause a framework strain that will affect the energy in a different way than the Ge incorporation energy described in the above paragraph. The graphic in Figure 9 shows that a linear correlation is observed when plotting the relative total energy versus the number of Ge−O−Ge linkages present in the corresponding distribution. This means that Ge atoms, from an energetic viewpoint, tends to locate far from each other. The slope of the straight line in Figure 9 may be an approximation to an energetic penalty per Ge−O−Ge linkage, and the value obtained is around 20 kJ/mol. Obviously, a different value may be obtained when calculating other configurations, and this value will have a contribution from the fact that the energetics of Ge in T1 and T1′ are not exactly the same (see Table S4); therefore, this should be taken as a first approximation. Theoretical calculations indicate that the substitution of Ge by Si at T3 sites is not energetically favored in ITQ-21.

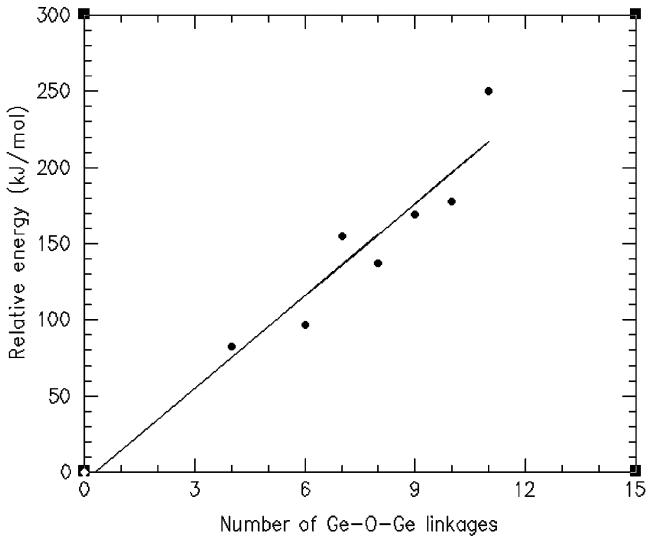

Figure 9. Energy of configurations generated with 12 Ge atoms distributed randomly in T1 and T1′ positions plotted against the number of Ge−O−Ge linkages that appear in the configuration. The unit cell composition is $Ge_{12}Si_{24}O_{72}$.

ITQ-21 shows a different behavior with respect to that observed for Ge containing ITQ-7 and ITQ-17 zeolites. Indeed, T3 remains a pure silica even at Si/Ge ratios lower than 2, while T1 and T2 sites are approaching a Si/Ge ratio close to 1 (see Tables 5 and 8). Even more, ^{19}F-MAS NMR data point toward the formation of some D4R cages with Si/Ge lower than 1, as deduced from the appearance of a signal at −14 ppm in the NMR spectrum. These results can be nicely explained by considering the calculated T-site energies involved for an hypothetical process of Ge incorporation into the ITQ-21 framework. At the beginning, at low Ge content, it is clear that Ge incorporation will be strongly directed toward T1 (and T1′) sites, due to the much lower energies of this position than for T2 and T3. This will be the favored Ge incorporation mechanism up to an upper limit of 50% occupancy of the T1 sites (i.e. $(Si/Ge)_{solid} = 2$). Above this loading, Ge will prefer to be placed at T2 sites, since further incorporation of Ge in T1 positions will lead to the formation of three Ge−O−Ge linkages (see Figure S6, given as Supporting Information), which as has been stated above produces an energetic penalty of approximately 20 kJ/mol per Ge−O−Ge moiety (i.e. each Ge in T1 sites will destabilize ITQ-21 by approximately 60 kJ/mol). In this situation, the most favored positions will be T2, that requires only 46.3 kJ/mol without forming any Ge−O−Ge linkage. Ideally, Ge incorporation can go ahead up to an upper limit of 50% occupation by Ge in T2 and T1 (and T1′) sites, while maintaining T3 as a pure siliceous position due to its huge energetic penalty (78.4 kJ/mol). The observed Ge distribution

among the different T sites in the 1.7Ge-ITQ-21 sample from the Rietveld refinement (see Table 5) is very close to these occupation values, and in this situation, only a small fraction of Ge seems to be involved in Ge−O−Ge linkages, as deduced from the low intensity of the −14 ppm resonance in the ^{19}F-MAS NMR spectrum. Nevertheless, the presence of this NMR signal gives strong experimental support to the calculated strong energetic penalty for placing Ge in T3 positions. Indeed, Ge prefers to be placed at D4R cages with a Si/Ge ratio lower than 1, with a consequent energy penalty of 60 kJ/mol, than to be located at T3 sites.

Conclusions

We have seen that it is possible to synthesize ITQ-21 in a wide range of Si/Ge and T^{IV}/T^{III} ratios. Germanium plays an important role in the nucleation step, up to the point that no induction period in the crystallization curve is observed at the times and temperatures studied here. In some cases, 100% crystallinity was obtained only after 6 h of crystallization.

When the Ge content is decreased in the gel, CIT-5 (which was also obtained with *N*-methylsparteinium as SDA) starts to compete with ITQ-21. However, it is possible to avoid such competition by working with more concentrated gels that favor the formation of zeolites with lower framework density. In an analogous way, Al incorporation into the synthesis gel and, consequently, the introduction of negative framework charges require a larger amount of organic cations to compensate them, favoring the formation of ITQ-21 versus CIT-5, with smaller void volume.

It is possible to fine-tune the crystallite size of ITQ-21 from nanocrystals (∼80 nm) to large crystals (∼2 μm) by controlling the relative rates of nucleation and crystal growth, through the H_2O/T^{IV} ratio. This should have important implications for ITQ-21 use in catalysis, electronics, and optics.

ITQ-21 zeolite samples present high thermal and hydrothermal stability when the Si/Ge ratio is above 10.

Ge preferentially occupies the T1 positions, located in the D4R, and, only for samples with a Si/Ge ratio below 4.5, T2 positions are also occupied. However, T3 positions remain purely siliceous, even for Si/Ge ratios as low as 1.7. This forces the formation of some Ge−O−Ge bonds. The above Ge distribution was confirmed by ^{19}F NMR MAS spectroscopy, which shows the presence of a band at −14 ppm, associated with the presence of Ge−O−Ge in Ge-rich D4R cages.

Computer simulations confirm that the lowest energetic configuration is achieved when Ge occupies T1 positions, followed by T2 position occupation. A larger substitution impediment is observed for Ge in T3 positions, with a high incorporation energy (78 kJ/mol), even larger than that required to form Ge−O−Ge pairs. Therefore, computer modeling gives theoretical support to the observed nonoccupation of the T3 position by Ge atoms and the formation of Ge−O−Ge bonds in ITQ-21 samples with very low Si/Ge ratios (≤2).

Acknowledgment. We thank the CICYT (projects MAT 2003-07945-C02-01 and MAT 2003-07769-C02-01) for financial support. We also thank Dr. Jose Luis Jordá for helpful contributions to the structural characterization.

Supporting Information Available: Crystallographic information (atomic coordinates, distances, and bond angles) of the ITQ-21 structure, crystallization curves, SEM images, DRX patterns, and NMR spectra; crystallographic data area also given as CIF files. This material is available free of charge via the Internet at http://pubs.acs.org.

JA047990Z